Video Article

Assessment of Boron Doped Diamond Electrode Quality and Application to *In Situ* Modification of Local pH by Water Electrolysis

Tania L. Read[1], Julie V. Macpherson[1]

[1]Warwick Electrochemistry and Interfaces Group, Department of Chemistry, University of Warwick

Correspondence to: Julie V. Macpherson at J.MacPherson@warwick.ac.uk

URL: https://www.jove.com/video/53484
DOI: doi:10.3791/53484

Keywords: Chemistry, Issue 107, Boron doped diamond, characterization, electroanalysis, electrochemistry, pH, sensors

Date Published: 1/6/2016

Citation: Read, T.L., Macpherson, J.V. Assessment of Boron Doped Diamond Electrode Quality and Application to *In Situ* Modification of Local pH by Water Electrolysis. *J. Vis. Exp.* (107), e53484, doi:10.3791/53484 (2016).

Abstract

Boron doped diamond (BDD) electrodes have shown considerable promise as an electrode material where many of their reported properties such as extended solvent window, low background currents, corrosion resistance, *etc.,* arise from the catalytically inert nature of the surface. However, if during the growth process, non-diamond-carbon (NDC) becomes incorporated into the electrode matrix, the electrochemical properties will change as the surface becomes more catalytically active. As such it is important that the electrochemist is aware of the quality and resulting key electrochemical properties of the BDD electrode prior to use. This paper describes a series of characterization steps, including Raman microscopy, capacitance, solvent window and redox electrochemistry, to ascertain whether the BDD electrode contains negligible NDC *i.e.* negligible sp^2 carbon. One application is highlighted which takes advantage of the catalytically inert and corrosion resistant nature of an NDC-free surface *i.e.* stable and quantifiable local proton and hydroxide production due to water electrolysis at a BDD electrode. An approach to measuring the local pH change induced by water electrolysis using iridium oxide coated BDD electrodes is also described in detail.

Video Link

The video component of this article can be found at https://www.jove.com/video/53484/

Introduction

Choice of electrode material is of great importance when conducting any electroanalytical study. In recent years, sp^3 carbon (diamond) doped with sufficient boron to render the material "metal-like" has become a popular choice for a wide range of electroanalytical applications due to its excellent electrochemical (and thermal and mechanical) properties[1,2,3]. These include corrosion resistance under extreme solution, temperature and pressure conditions[4] ultra-wide solvent windows, low background currents, and reduced fouling, in comparison to other commonly used electrode materials[5-7,3]. However, increasing non-diamond-carbon (NDC: sp^2) content results in a decreasing solvent window, increasing background currents[7,8], changes in both structural integrity and sensitivity towards different inner sphere redox species, *e.g.* oxygen[9-12].

Note for some applications, NDC presence is seen as advantageous[13]. Furthermore, if the material does not contain sufficient boron it will behave as a p-type semi-conductor and show reduced sensitivity to redox species in the reductive potential window, where the material is most depleted of charge carriers[7]. Finally, the surface chemistry of boron doped diamond (BDD) can also play a role in the observed electrochemical response. This is especially true for inner sphere species which are sensitive to surface chemistry and lower doped diamond where a hydrogen (H-)-terminated surface may make a semi-conducting BDD electrode appear "metal-like"[7].

To take advantage of the superior properties of BDD, it is often essential the material is sufficiently doped and contains as little NDC as possible. Dependent on the method adopted to grow the BDD, the properties can vary[14,15]. This paper first suggests a materials and an electrochemical characterization protocol guide for assessing BDD electrode suitability prior to use (*i.e.* sufficient boron, minimal NDC) and then describes one application based on locally changing pH electrochemically using the protocol-verified electrode. This process takes advantage of the surface resilience of NDC-free BDD towards corrosion or dissolution under application of extreme applied potentials (or currents) for long periods of time. In particular the use of a BDD electrode to generate stable proton (H^+) or hydroxide (OH^-) fluxes due to electrolysis (oxidation or reduction respectively) of water in close proximity to a second (sensor)[16,17] is described herein.

In this way it is possible to control the pH environment of the sensor in a systematic way, *e.g.* for pH titration experiments, or to fix the pH at a value where the electrochemical process is most sensitive. The latter is especially useful for applications where the sensor is placed at the source, *e.g.* river, lake, sea and the pH of the system is not optimal for the electrochemical measurement of interest. Two recent examples include: (i) generation of a localized low pH, in a pH neutral solution, for the electrodeposition and stripping of mercury[17]; note BDD is a favored material for electrodeposition of metals due to the extended cathodic window[9,18,19]. (ii) Quantification of the electrochemically detectable form of hydrogen sulfide, present at high pH, by locally increasing the pH from neutral to strongly alkaline[16].

Protocol

NOTE: BDD electrodes are most commonly grown using chemical vapor deposition techniques, attached to a growth substrate. They leave the growth chamber H-terminated (hydrophobic). If grown thick enough the BDD can be removed from the substrate and is termed freestanding. The freestanding BDD growth surface is often polished to significantly reduce surface roughness. Cleaning the BDD in acid results in an oxygen (O)-terminated surface.

1. Acid Cleaning BDD

1. Place a beaker of concentrated sulfuric acid (H_2SO_4; ~ 2 ml or deep enough to cover the diamond) on a hot plate at RT and insert the BDD.
2. Add potassium nitrate (KNO_3) until it no longer dissolves (~ 0.5 g in 2 ml), then cover with a watch glass and heat to ~ 300 °C, the solution will turn brown as it heats and the potassium nitrate will dissolve.
   CAUTION! Care should be taken when handling hot acid; rubber gloves, safety glasses and lab coat should be worn and this process should be conducted in a fume hood.
3. Leave to heat for at least 30 min or until there is no longer any brown color to the solution, then turn off the hot plate and leave the solution to cool to RT.
4. Carefully dispose of the acid by diluting in RT water and rinse the BDD with distilled water.
5. Measure the surface contact angle, see section 1.2. Hydrophobic (H-terminated)[20,21] electrodes have reported contact angles in the range 60-90°[3], which significantly reduces as the surface is rendered hydrophilic through O-termination.
6. (optional alternative method) For very thin film electrodes (attached to the growth substrate and to avoid film delamination using the above treatment), wash once with 2-propanol and twice with deionized water in an ultrasonic bath. Then, adopt one of the following three cleaning procedures (1) anodically polarize the diamond for 30 min at 10 mA cm^{-2} in 1 M perchloric acid at 40 °C[22]; or (2) anodically polarize the diamond for 20 min at 10 mA cm^{-2} in 1 M nitric acid, then subsequently cathodically polarize at 10 mA cm^{-2} for a further 20 min in the same solution[23] or; (3) cycle the diamond between 2 V in 0.1 M H_2SO_4 until a stable electrochemical signal is achieved[7]. Follow this with step 1.4.

2. Contact Angle Measurement

1. Place the diamond on the sample stage of a contact angle analyzer, ensuring it is flat. Place a 1 ml syringe in the positioner above the sample stage, secure a needle on the end. Fill the syringe with deionized water.
2. Use the z-controller to lower the syringe to the sample, use the *x*- and *y*- controllers and the camera/illuminator to align the syringe above the center of the diamond.
3. Using the analyzer software dispense repeat 1 µl volumes of water out of the syringe until a droplet forms at the tip of the needle, visible on the camera image (never more than 10 µl). Lower the needle to deposit the droplet on to the surface and adjust the illumination for maximum contrast.
4. Collect an image and apply drop shape analysis software, using the conic section method. Click "find baseline" in the software, and then click "computation" followed by "tangent".
   NOTE: this procedure detects the baseline and fits a conic equation to the (elliptical) drop shape; a contact angle, θ, is drawn between the baseline and the tangent at the three-phase contact point.

3. BDD Material Characterization

1. Raman Analysis for sp^2/sp^3 content
   1. Carry out Raman (see reference[14] for a guide to Practical Raman Spectroscopy) in several different areas of the BDD electrode,[24] use of a 514.5 nm or 532 nm laser, which emphasizes sp^2 content, is advocated.
   2. Turn on the micro-Raman spectrometer and allow ~30 min for the CCD Detector to cool down. Check the appropriate lens, diffraction grating and filters are in place for use with the laser of choice.
   3. Calibrate the system using a silicon (Si) calibration sample. Place the Si substrate in the instrument chamber and focus optically on the sample with the microscope. Shut the door to the chamber. Switch to laser view and check the laser spot is well defined and circular. Calibrate using the software, click "tools" followed by "calibration" then "quick calibration" then "ok".
   4. Remove the Si substrate from the chamber and replace with the BDD electrode. Optically focus the microscope on the area of interest, switch to laser view and open the shutter to check that the laser is focused. Close the shutter.
   5. Take a Raman measurement using the software; click "measurement" then "new" then "spectral acquisition." set the measurement wavenumber range to cover the features of interest, for BDD this is 200 - 1,800 cm^{-1}; set the scan acquisition time (<10 sec); set the laser power to 100% (for BDD) and; set the number of accumulations (repeat scans) to five (for BDD). If the resulting spectrum is very noisy more accumulations may be necessary. Press run and save the resulting spectrum for analysis. Take a picture of the area Raman was performed in using the live video. Save the image as a reference.
   6. Observe the peak ~ 1,332 cm^{-1} in the spectrum which indicates sp^3 diamond (**Figure 1**); the broader the peak the more defects present[3,25].
   7. Observe any NDC — indicated by a broad G peak centered at 1,575 cm^{-1} [26], in the spectra (**Figure 1A** and **1B**), originating from the stretching of paired sp^2 sites; the greater the peak intensity the more NDC present.
      NOTE: the π bonds formed by sp^2 C are more polarizable than sp^3 σ bonds and are resonantly enhanced by visible lasers, leading to broader, more dominant, G peaks[25]. Note that the exact method used to perform analyses may vary between different instruments and software.

4. Electrochemical Characterization

1. Preparing ohmic contacts
    1. Freestanding BDD
        1. Using standard techniques sputter (or evaporate)the backside of the BDD with titanium (Ti)/gold (Au) 10 nm/300 nm, using a sputterer/evaporator at pressures below 1 × 10^{-5} mBar. If a three target source is available, more ideally is Ti 10 nm / platinum (Pt) 10 nm / Au 300 nm to avoid diffusion of Ti into the Au.
        2. Anneal for 5 hr at 400 °C (atmospheric pressure) enabling the Ti to form titanium carbide, crucial for formation of an ohmic contact[27].
           NOTE: if the back surface of the BDD is highly polished (~ nm roughness) then it is preferably to roughen the surface prior to sputter deposition to ensure a more robust coating. This can be achieved by, for example, low power laser micromachining the surface (removing < 30 µm material).

    2. Thin film diamond grown on a conducting substrate
        1. Sputter/evaporate as above, but to the top face, using a shadow mask gently place on the top surface to avoid top contacting the entire electrode.
           OR
        2. Scratch the back of the conducting substrate using a diamond tipped pen. Then coat the scratched area with conducting Ag paste or a similar conductive paint by painting on a thin layer with a small paintbrush. Finally, electrically connect by attaching copper wires with conductive epoxy.
           NOTE: there are a variety of ways to prepare the BDD after electrical contact as described in reference 4, *e.g.* if the BDD can be machined into smaller structures, seal in glass or epoxy, or if still attached to the wafer clamp/attach an electrochemical cell to the top surface.

2. Capacitance Measurements
    1. Prepare a 20 ml of 0.1 M KNO_3 solution by weighing 0.20 g in doubly distilled water (this water quality is recommended throughout, resistivity 18.2 M cm). Clean the electrode prior to use either by alumina polishing or by electrochemically cycling in dilute acid (see section 1 NOTE)[16,23,28].
    2. Using a potentiostat run cyclic voltammograms (CVs) at 0.1 V sec^{-1} between -0.1 V and 0.1 V, starting at 0 V, with the BDD as the working electrode versus a common reference electrode, *e.g.* silver/silver chloride (Ag/AgCl) or a saturated calomel electrode (SCE), and a Pt counter electrode. Analyze the second CV.
       NOTE: **Figure 2A** shows a typical capacitance curve recorded with a freestanding metallic doped BDD electrode.
    3. Measure the total current magnitude at 0 V from the recorded capacitance curve and divide by 2, this value is "*i*". Determine the capacitance, *C*, using the value for *i*, with equation 1, normalize with respect to electrode area (accounting for surface roughness if appropriate) and quote in µF cm^{-2}. High quality, "metal-like" BDD has a capacitance << 10 µF cm^{-2}. Use any data plotting software to present and analyze the data.
       $i = C(Vt^{-1})$ (eq. 1);
       where *i* is current (A) and (V t^{-1}) is the potential scan rate.

3. Solvent Window
    1. Clean the electrode as in step 4.2.1. Using a potentiostat run a CV in 0.1 M KNO_3 at 0.1 V sec^{-1} from 0 V to -2 V then between -2 V and +2 V and back to 0 V with the BDD as the working electrode vs. a common reference electrode and Pt counter electrode. Repeat. Analyze the second CV, an example CV is shown in **Figure 2B**.
    2. Convert current to current density (mA cm^{-2}), taking surface roughness into account, and quote the solvent window as the potential window defined by current limits of ±0.4 mA cm^{-2} in both directions.[7,29] Use any data plotting software to present and analyze the data.
    3. Observe the evidence of NDC (sp^2 carbon) in the solvent window; the oxygen reduction reaction is favored on NDC that is clearly evident in the reductive window. Oxidation of sp^2 containing groups also results in characteristic peaks just before water electrolysis in the anodic window (**Figure 2B**).
       NOTE: high quality "metallic" BDD electrodes have solvent windows >> 3 V, do not support the oxygen reduction reaction (ORR) in 0.1 M KNO_3 (or ORR is strongly kinetically retarded) and show negligible NDC oxidation signatures.

4. Redox Electrochemistry
    1. Clean the electrode as in step 4.2.1.
    2. Using a potentiostat record CVs in 1 mM ruthenium hexaamine ($Ru(NH_3)_6^{3+}$) and 0.1 M KNO_3 between +0.2 V and -0.8 V versus SCE, for scan rates in the range 0.05 V sec^{-1} - 0.2 V sec^{-1}.
       NOTE: This couple shows fast electron transfer and is electroactive in a region which challenges p-type semiconducting BDD. sp^2 containing BDD will also show ORR in this region, the signal for the latter is more evident as the concentration of $Ru(NH_3)_6^{3+}$ is decreased.
    3. Measure the voltage separation between the anodic and cathodic peak current (ΔE_p) from the recorded CV, and the temperature as described[20]. For "metal-like" ohmically contacted oxygen-terminated BDD at 298 K, ΔE_p < 70 mV[30,31]. Larger ΔE_p values are symptomatic of a poor ohmic contact or a lower boron content, as shown in **Figure 2C** for BDD electrodes of dopant densities in the range 9.2 × 10^{16} to 3 × 10^{20} B atoms cm^{-3}.
    4. Measure the peak current of the forward scan, i_p, and correlate with that expected from the Randles Sevcik equation 2 (quoted at 298 K)[3,30], assuming the electrode is disk-shaped in geometry and large enough (diameter 1 mm) that linear diffusion dominates. Use any data plotting software to present and analyze the data.
       $i_p = 2.69 \times 10^5 n^{3/2} AD^{1/2} cv^{1/2}$ (eq 2)

where n is the number of electrons transferred, A is area (cm^2), D is diffusion coefficient (cm^2 sec^{-1}), c is concentration (mol cm^{-3}) and v is scan rate (V sec^{-1}).

5. pH Generation: Preparation of pH Sensitive Electrode and pH Generation

1. Iridium Oxide (pH sensitive) Solution Preparation
    1. Prepare a 20 ml 0.1 M KNO_3 solution as in section 5.4.1. Add 5 drops of phenolphthalein indicator solution using a Pasteur pipette and stir (this is sufficient to see a response by eye, but for a more intense color, add more drops). Place the BDD working electrode and Pt counter electrode in solution.
    2. Adjust pH of the solution to 10.5 by addition of anhydrous potassium chloride salt, stirring continuously. Leave covered and stirring for 48 hr at RT to stabilize, at this stage the solution will gradually go from yellow-green to blue-purple. Store in a refrigerator at 3 °C.

2. pH Sensitive Iridium Oxide Film Deposition
    1. Using a potentiostat run a CV in the iridium oxide solution between 0 V and +1 V versus SCE to determine the potential at which the maximum current is recorded. This is the deposition potential, E_{dep} as shown in **Figure 3A**, typically lying between ~+0.6 V – +0.85 V; it can vary depending on a number of factors such as temperature, electrode material *etc.*[32,33]
    2. Using chronoamperometry with a potentiostat, step the potential from 0 V ("initial E" and "Low E" in the software), where no electrolysis occurs to E_{dep} ("High E" in the software), for a time period of 0.2 sec per step, repeat 100x.
    3. Run a CV between 0 V and +1 V in 0.1 M H_2SO_4 for the IrO_x deposited electrode. The characteristic CV shape is shown in **Figure 3B**. A current density in the range ~ 0.6 mA cm^{-2} - 0.7 mA cm^{-2} for the first anodic peak (corresponding to an average film thickness of ~ 8 nm for 0.7 mA cm^{-2}), indicates a stable pH sensitive film[34,35].
    4. If the current density is less than 0.6 mA cm^{-2} repeat steps 5.2.2 - 5.2.4 until this value is reached. Leave the electrode in pH 7 buffer solution for 24 hr to hydrate as the response of the IrO_x film is hydration-dependant[33].

3. IrO_x Film pH Characterization
    1. Prepare a series of buffer solutions which cover the pH range of interest (pH 2 - pH 12), these can be made in house (*e.g.* Carmody[36]) or purchased commercially.
    2. Rinse the electrode with distilled water. Place the IrO_x electrode and reference electrode in the buffer solution of lowest pH. Using a potentiostat record the open circuit potential (OCP) over 30 sec, with three repeats. Remove the electrode from the solution, rinse and place in the next buffer.
    3. Repeat step 5.3.2 for each buffer, then repeat the series at least twice. Plot pH vs. OCP, the calibration plot for the film response. An IrO_x film exhibits a slope with a gradient between 59 - 80 mV per decade[37].
    NOTE: **Figure 3C** shows an example calibration plot for a successful IrO_x pH sensor on BDD.

4. Using a pH generator and measurement system
NOTE: this assumes use of a dual electrode system where one electrode is coated with the IrO_x film (*e.g.* disc) and the second (*e.g.* BDD ring) will generate H^+ or OH^- galvanostatically from water electrolysis.
    1. Prepare a 20 ml 0.1 M KNO_3 solution by adding deionized water to the salt. Connect the IrO_x coated electrode as the working electrode in a two electrode system, with the second electrode a stable reference electrode *e.g.* SCE. Measure the OCP using a potentiostat, to establish the starting pH.
    2. Connect the generator electrode to a suitable two electrode galvanostatic system with a counter electrode, *e.g.* Pt foil, and repeat step 5.4.1, but after a defined period of time apply a current to the generator electrode.
    NOTE: we find currents in the range 0 to ± 50 µA are suitable with our BDD electrodes; larger currents result in appreciable gas evolution. The magnitude and direction of the current depends on the desired result; a positive current will result in a shift to more acidic pH and a negative current to more alkaline pH, the larger the current the greater the pH change.
    3. Using the potentiostat, record the change in OCP in response to the galvanostatic current, wait until the response stabilizes. Then place the IrO_x electrode in pH 7 buffer for 10 min to re-equilibrate the IrO_x film.
    4. Repeat steps 5.4.2 to 5.4.3 with different applied currents, until all the data required has been collected. Plot the data using the calibration curve obtained in section 5.3 to convert OCP to pH, an example data set is shown in **Figure 4A**. Remove the IrO_x film using alumina polishing or pulsing in 0.1 M H_2SO_4 from +2 V to -2 V for 0.2 sec, ×100. Apply to the measurement system of interest.

5. Visual assessment of local pH generation
    1. Prepare a 20 ml 0.1 M KNO_3 solution as in section 5.4.1. Add 5 drops of phenolphthalein indicator solution using a Pasteur pipette and stir (this is sufficient to see a response by eye, but for a more intense color, add more drops). Place the BDD working electrode and Pt counter electrode in solution.
    2. Apply a negative current to the working electrode using a galvanostat as in step 5.4.2 (*e.g.* ~ -0.6 mA cm^{-2}) such that the solution changes color from colorless to pink. This now locally generates a solution which is at pH ≥ 10.5.
    3. Repeat step 5.5.1 with 5 drops of methyl red solution instead of phenolphthalein and stir. Apply a sufficiently positive current (*e.g.* ~ 6.6 mA cm^{-2}) such that the solution changes color from yellow to red. This now locally generates a solution which is at pH ≤ 4.2[38].

Representative Results

Raman spectra and electrochemical characteristics were obtained for representative BDD macrodisc electrodes with different dopant densities, and both significant and negligible levels of NDC, **Figures 1** and **2**. **Figures 1A** and **B** show typical Raman data for NDC-containing thin film microcrystalline BDD and larger grain freestanding BDD, doped above the metallic threshold, respectively. The presence of NDC is identifiable by the labeled broad peaks between 1,400 and 1,600 cm^{-1}; there is no such peak visible in **Figure 1C**, which shows the typical Raman signature of NDC-free, freestanding BDD. In all three spectra in **Figure 1** it is possible to observe a sharp peak at 1,332 cm^{-1}, this is the signature peak of sp^3 carbon (diamond); asymmetry of the baseline around this peak is known as a "Fano resonance" and if present indicates that the sample is suitably doped (10^{20} B atoms cm^{-3}) for use in electrochemical studies. This is the case for all three electrodes shown here.

In **Figure 2** example data for electrochemical studies (capacitance, solvent window and CVs recorded in the redox mediator $Ru(NH_3)_6^{3+}$) are presented for both NDC-containing and NDC-free BDD, doped above the metallic threshold. The capacitance curves in **Figure 2A** clearly indicate that NDC-containing BDD exhibits a greater capacitive current than NDC-free BDD. The capacitances for each has been calculated as described in the text and are quoted in **Figure 2A** as 10.8 μF cm^{-2} (NDC-containing) and 6.3 μF cm^{-2} (NDC-free) BDD. High quality, low NDC-content, BDD electrodes are expected to have a capacitance <<10 μF cm^{-2}. Similarly, **Figure 2B** compares the solvent windows of exemplar NDC-containing and NDC-free BDD electrodes. It can be seen that for an NDC-containing electrode the onset of H_2O oxidation and reduction has been brought in significantly, narrowing the solvent window. Also of note is the appearance of anodic peaks due to the oxidation of NDC and a cathodic peak due to ORR which is catalyzed on NDC but not on sp^3 carbon. For a high quality BDD electrode with negligible NDC the solvent window is expected to be >>3 V in aqueous KNO_3 solution. In **Figure 2C** the CV response of BDD electrodes with a variety of doping levels are investigated using the redox mediator $Ru(NH_3)_6^{3+}$. For BDD electrodes doped above the metallic threshold, the voltage separation between the anodic and cathodic current peaks is expected to be close to 59 mV, in accordance with the Nernst equation; however, as the dopant level decreases the material becomes depleted of charge carriers resulting in an increase in the peak to peak separation.

A BDD macrodisc, coated in IrO_x, was used to record the data in **Figure 3**, while all diamond (BDD insulated in diamond)[39] dual electrodes and an epoxy sealed BDD ring disc electrode were used for the pH generation experiments in **Figure 4A**. The data in **Figure 3** illustrates the deposition and characterization process for a pH sensitive IrO_x film on BDD. In **Figure 3A** a typical CV recorded in the IrO_x deposition solution is shown. The potential employed for subsequent IrO_x deposition can be identified from the position of the oxidative current peak, as illustrated here. **Figure 3B** is an exemplar CV in sulfuric acid of an IrO_x film electrodeposited on BDD. The shape of the CV is characteristic of a successfully deposited film with the peak current density providing information on film thickness. A higher current density indicates a thicker film. The stability of the film is thickness dependent; too thin and the pH response will drift, too thick and the film response time will be slow and the film can flake off. A value for peak current density ~0.7 mA cm^{-2} has been shown to indicate a stable film with an excellent pH response. The OCP response of the IrO_x layer on a BDD electrode towards different pH buffers is shown in **Figure 3C**. The drift between measurements is small as evidenced by the size of the error bars and the slope is super-Nernstian (>59 mV) as expected for this type of film.

Finally, **Figure 4** illustrates the use of a BDD electrode for pH generation. In **Figure 4A** the pH change measured at an IrO_x coated BDD electrode is presented for a range of currents applied to the pH generation BDD electrode placed nearby, either in ring or band format, as illustrated in **Figure 4**. For different applied currents, the pH can be changed locally and quantifiably from a starting value (near neutral) to either acidic or alkaline. This process can be observed visually as illustrated in **Figure 4B**, where a suitable current density is applied to a BDD electrode to change the pH from close to neutral to >10.5. In the presence of phenolphthalein (pH indicator) this results in the solution going from colorless to pink, in the vicinity of the electrode.

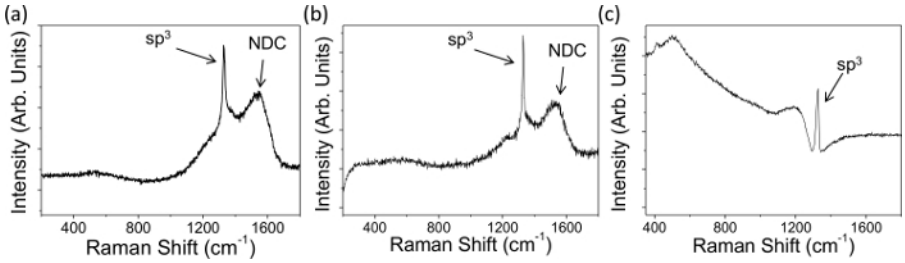

Figure 1. Typical Raman data recorded with a 514 nm laser on (A) NDC containing thin film microcrystalline BDD attached to the growth substrate (dopant density 1.9 × 10^{20} boron atoms cm^{-3}) and (B, C) larger grain freestanding BDD, average dopant density 1.9 × 10^{20} and 3 × 10^{20} B atoms cm^{-3} respectively. NDC is evident in (**A**) and (**B**) due to the presence of the labeled NDC peaks between 1,400 and 1,600 cm^{-1}, (**C**) contains negligible NDC. All three electrodes show a "Fano resonance" and thus are suitably boron doped for electrochemical studies[7]. Reproduced in part from reference [4c] with permission. Please click here to view a larger version of this figure.

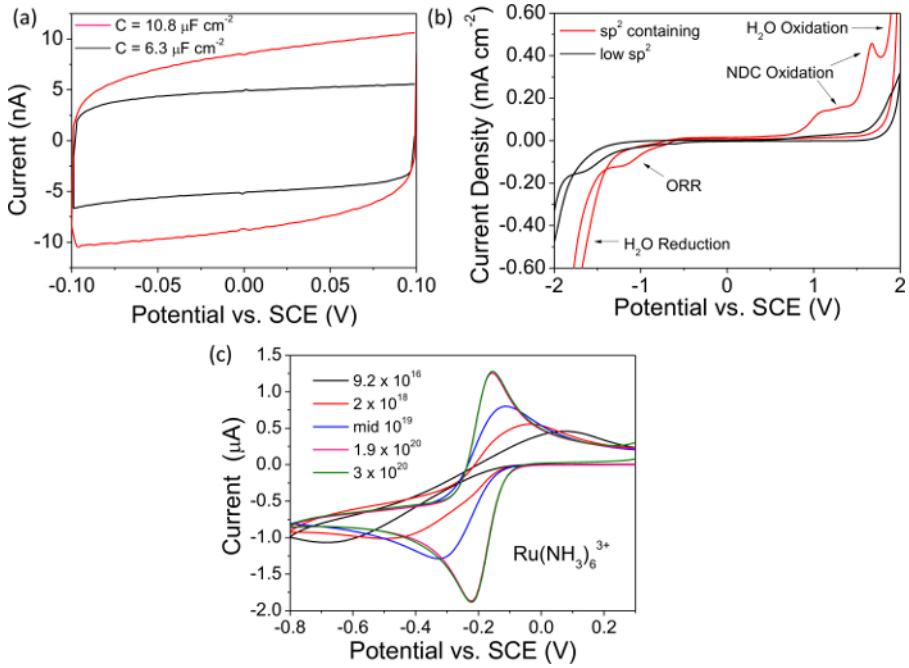

Figure 2. Electrochemical characterization. All representative data in (**A**, **B**) has been recorded on insulating diamond encased O-terminated BDD electrodes doped above the metallic threshold *i.e.* 10^{20} B atoms cm^{-3}[39]. (**A**) Capacitance curves for NDC-free BDD where C = 6.3 μF cm^{-2} (**black**), and for NDC-containing BDD where C = 10.8 μF cm^{-2} (**red**). (**B**) Representative solvent windows for NDC-free BDD, solvent window > 3.95 V (**black**) and for NDC-containing BDD, solvent window = 3.22 V (**red**). (**C**) CVs recorded in 1 mM $Ru(NH_3)_6^{3+}$ at 0.1 V sec^{-1} for glass sealed freestanding BDD macrodisc electrodes of different boron dopant densities in the range 9.2 × 10^{16} - 3 × 10^{20} B atoms cm^{-3}. Reproduced in part from reference [4c] with permission. Please click here to view a larger version of this figure.

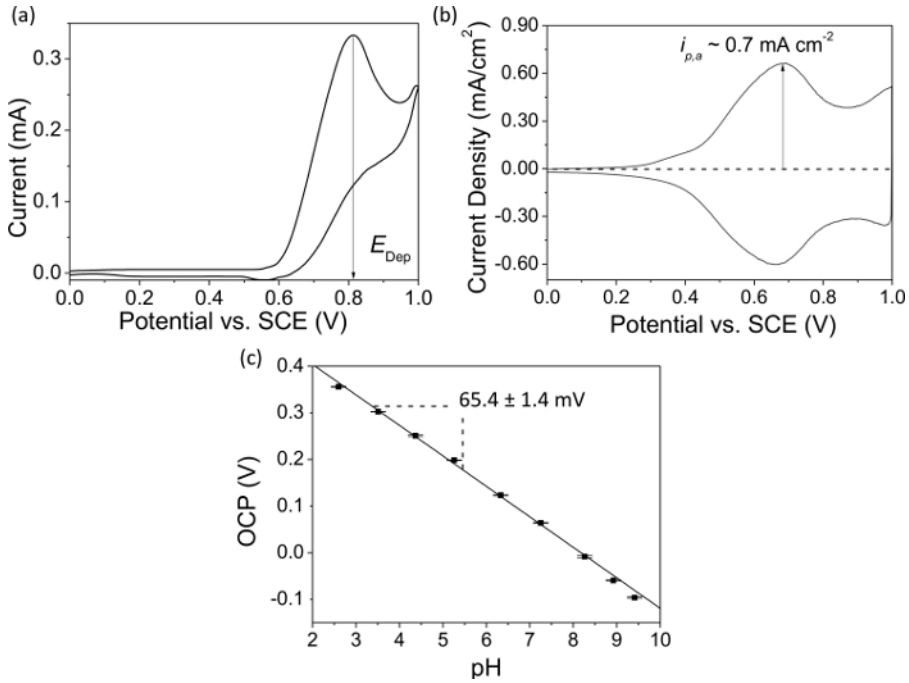

Figure 3. Characterization of IrO_x film deposition on BDD and pH response. (**A**) CV in IrO_x solution prior to deposition. The maximum oxidation current provides a value for the deposition potential, E_{dep}, where film formation is found to be most efficient. Using potentials > E_{dep}, results in an unstable deposited film. (**B**) Characteristic CV for an electrodeposited IrO_x film in 0.1 M H_2SO_4 recorded at 0.1 V sec^{-1}; $i_{p,a}$ is typically ~ 0.7 mA cm^{-2}. (**C**) Representative pH calibration curve (R^2 = 0.997) for electrodeposited IrO_x on a freestanding BDD electrode. The slope shows a super-Nernstian response (65.4 mV) to pH. The small error bars (n=3) indicate film stability and reproducibility in the measurements. Please click here to view a larger version of this figure.

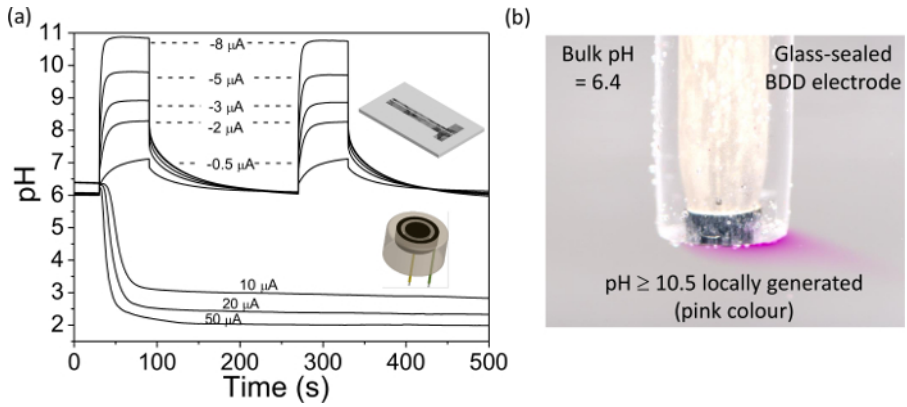

Figure 4. Use of a freestanding BDD ring disc and dual band electrodes for *in situ* pH control. BDD ring disc electrode, disc diameter = 0.922 mm, separation = 0.262 mm, and ring width = 0.150 mm; BDD band electrode generator = 0.460 × 3 mm, detector = 0.09 × 3 mm, and separation = 0.2 mm. (**A**) Experimentally measured pH versus time profile over the detector electrodes as a function of applied galvanostatic current (+10 to +50 µA at the ring disc electrode and -0.5 to -8 µA for the dual band electrode). Note the stable pH generated over long periods of time. Modified reproduction of references [9a] and [9b]. (**B**) Simple visualization of *in situ* pH generation using phenolphthalein indicator solution; a current of -4.55 µA (-0.58 mA cm^{-2}) was applied to a 1 mm diameter glass sealed BDD macroelectrode. The pink color indicates pH≥10.5, colorless solution indicates pH≤8.4 [38]. Please click here to view a larger version of this figure.

Discussion

Starting with an O-terminated surface is advocated because the H-terminated surface is electrochemically unstable, especially at high anodic potentials[7,40,41]. Changing surface termination can affect the electron transfer kinetics of inner sphere couples, such as water electrolysis (used herein to change the local solution pH). Furthermore, if the BDD contains significant NDC at grain boundaries it is also possible that upon application of the extreme anodic/cathodic potentials advocated in this article for pH generation, etching could occur at these weaker points. This would cause the film to corrode and for thin films, eventually delaminate, manifesting itself in an unstable pH generation profile, as seen with thin film Au and Pt electrodes[17]. Hence a stringent protocol for assessing the quality of the electrode prior to use is adopted to assess NDC content as discussed in **Figures 1** (Raman) and **2** (capacitance and solvent window).

Also of importance is the boron content. If the material is doped below the metallic threshold (< 10^{20} B atoms cm^{-3}), it will be charge depleted, at potentials negative of the flatband potential, resulting in a decrease in electrochemical performance[7,42]. The easiest way to qualitatively assess metallic doping levels is to look for the presence of a Fano signature which causes asymmetry in the sp^3 peak, in the Raman spectra, as shown in **Figure 1(A-C)**. This is due to interference between the discrete phonon state and the electronic continuum and is seen at boron doping levels > 10^{20} B atoms cm^{-3}[43]. Secondary ion mass spectrometry (SIMS) ultimately quantifies boron content but is destructive and more intensive to use. Note as SIMS provides total boron content it does not account for possible reductions in the number of freely available charge carriers due to compensation or passivation of boron acceptors with suitable donors such as nitrogen[44] or hydrogen[45] respectively.

Electrochemically, dopant density differences can be visualized by employment of an outer sphere fast electron transfer redox couple whose formal potential lies within the band-gap of O-terminated semi-conducting BDD, such as $Ru(NH_3)_6^{3+/2+}$ [46]. For example, as shown in **Figure 2C**, as the doping levels of the BDD electrode increase, and the material moves from semi-conducting to metallic the current increases and the peak to peak separation decreases as electron transfer becomes more facile. At metallic dopant levels the electrode should show behavior similar to a classical electrode where for a mediator such as $Ru(NH_3)_6^{3+}$, reversible diffusion limited CVs are recorded at a macroelectrode in stationary solution. Note, at boron dopant levels ~ 10^{19} close to reversible behavior has been recorded but only for H-terminated surfaces. This is due to an interesting peculiarity of this surface where H-terminated causes the energy levels of the valence and conduction bands in diamond to be raised. This means electron transfer from the valence band to H_3O^+ is now possible, resulting in surface transfer doping and a measurable surface conductivity. However, due to the electrochemical instability of the H-terminated surface, especially at high anodic potentials, working with H-terminated lower dopant density electrodes is not a long-term viable approach[7,40,41].

The ability to modify the local pH of the measurement electrode has many different applications, for example local pH titration experiments now become possible where the pH can be systematically modified and the impact on the system electrochemically assessed *in situ*. Bound metal ions can be freed by decreasing pH enabling the sensor electrode to both assess free metal content at the natural pH and total metal content by locally decreasing to very acidic values, *in situ*[47-50]. This is very useful for at the source measurements. Additionally, species can be switched from not being electrochemically detectable to detectable by virtue of changing the local pH, *e.g.* dissolved hydrogen sulfide completely converts to the electrochemically detectable sulfide form at pH values > 9 [16]. In the example given, for the electrode geometries employed, pH changes over 4 units (from 6.4 to 2.0 and 6.0 to 10.8) were demonstrated. Larger changes are possible by increasing the galvanostatic current and changing the electrode geometries. For example, decreasing the separation between the generator and detector electrodes and reducing the relative size of the detector will allow lower/higher pH values to be attained. The feature size of the BDD electrode will be limited by the resolution of the fabrication technique employed. Note, there is also an upper limit to the size of the current able to be passed for stable pH generation. This is dictated by the current at which significant gas evolution and bubble formation at the generating electrode is observed.

Disclosures

The authors declare that they have no competing financial interests.

Acknowledgements

We would like to thank Dr. Jonathan Newland for the photograph in **Figure 4B** and for processing optical microscope images for the video, Miss Jennifer Webb for advice and visuals on contact angle measurements, Miss Sze-yin Tan for the solvent window data in **Figure 2B**, Dr Maxim Joseph for advice on Raman spectroscopy, and also members of the Warwick Electrochemistry and Interfaces Group who have helped to develop the protocols described herein. We would also like to thank Max Joseph, Lingcong Meng, Zoe Ayres and Roy Meyler for their part in filming the protocol.

References

1. Angus, J. C. Electrochemistry on diamond: History and current status. *Synthetic Diamond Films: Preparation, Electrochemistry, Characterization and Applications.* (eds. E. Brillas & C.A.M. Huitle) Ch. 1, John Wiley & Sons, Inc. (2011).
2. Fujishima, A. *Diamond Electrochemistry.* BKC. (2005).
3. Macpherson, J. V. A practical guide to using boron doped diamond in electrochemical research. *Physical Chemistry Chemical Physics.* **17** (5), 2935-2949 (2015).
4. Balmer, R. S. *et al.* Chemical vapour deposition synthetic diamond: materials, technology and applications. *Journal of Physics: Condensed Matter.* **21** (36), 364221 (2009).
5. Swain, G. M., & Ramesham, R. The electrochemical activity of boron-doped polycrystalline diamond thin film electrodes. *Analytical Chemistry.* **65** (4), 345-351 (1993).
6. Luong, J. H. T., Male, K. B., & Glennon, J. D. Boron-doped diamond electrode: synthesis, characterization, functionalization and analytical applications. *Analyst.* **134** (10), 1965-1979 (2009).
7. Hutton, L. A. *et al.* Examination of the Factors Affecting the Electrochemical Performance of Oxygen-Terminated Polycrystalline Boron-Doped Diamond Electrodes. *Analytical Chemistry.* **85** (15), 7230-7240 (2013).
8. Bennett, J. A., Wang, J., Show, Y., & Swain, G. M. Effect of sp2-Bonded Nondiamond Carbon Impurity on the Response of Boron-Doped Polycrystalline Diamond Thin-Film Electrodes. *Journal of The Electrochemical Society.* **151** (9), E306-E313 (2004).
9. Martin, H. B., Argoitia, A., Landau, U., Anderson, A. B., & Angus, J. C. Hydrogen and Oxygen Evolution on Boron-Doped Diamond Electrodes. *Journal of The Electrochemical Society.* **143** (6), L133-L136 (1996).
10. Panizza, M., & Cerisola, G. Application of diamond electrodes to electrochemical processes. *Electrochimica Acta.* **51** (2), 191-199 (2005).
11. Williams, O. A. Nanocrystalline diamond. *Diamond and Related Materials.* **20** (5-6), 621-640 (2011).
12. Patel, A. N., Tan, S.-y., Miller, T. S., Macpherson, J. V., & Unwin, P. R. Comparison and Reappraisal of Carbon Electrodes for the Voltammetric Detection of Dopamine. *Analytical Chemistry.* **85** (24), 11755-11764 (2013).
13. Watanabe, T., Honda, Y., Kanda, K., & Einaga, Y. Tailored design of boron-doped diamond electrodes for various electrochemical applications with boron-doping level and sp2-bonded carbon impurities. *physica status solidi (a).* **211** (12), 2709-2717 (2014).
14. Poferl, D. J., Gardner, N. C., & Angus, J. C. Growth of boron-doped diamond seed crystals by vapor deposition. *Journal of Applied Physics.* **44** (4), 1428-1434 (1973).
15. Spitsyn, B. V., Bouilov, L. L., & Derjaguin, B. V. Vapor growth of diamond on diamond and other surfaces. *Journal of Crystal Growth.* **52, Part 1**, 219-226 (1981).
16. Bitziou, E. *et al. In Situ* Optimization of pH for Parts-Per-Billion Electrochemical Detection of Dissolved Hydrogen Sulfide Using Boron Doped Diamond Flow Electrodes. *Analytical Chemistry.* **86** (21), 10834-10840 (2014).
17. Read, T. L., Bitziou, E., Joseph, M. B., & Macpherson, J. V. *In Situ* Control of Local pH Using a Boron Doped Diamond Ring Disk Electrode: Optimizing Heavy Metal (Mercury) Detection. *Analytical Chemistry.* **86** (1), 367-371 (2014).
18. Manivannan, A., Tryk, D., & Fujishima, A. Detection of Trace Lead at Boron-Doped Diamond Electrodes by Anodic Stripping Analysis. *Electrochemical and solid-state letters.* **2** (9), 455-456 (1999).
19. Manivannan, A., Seehra, M. S., Tryk, D. A., & Fujishima, A. Electrochemical detection of ionic mercury at boron-doped diamond electrodes. *Analytical Letters.* **35** (2), 355-368 (2002).
20. Boukherroub, R. *et al.* Photochemical oxidation of hydrogenated boron-doped diamond surfaces. *Electrochemistry Communications.* **7** (9), 937-940 (2005).
21. Yagi, I., Notsu, H., Kondo, T., Tryk, D. A., & Fujishima, A. Electrochemical selectivity for redox systems at oxygen-terminated diamond electrodes. *Journal of Electroanalytical Chemistry.* **473** (1), 173-178 (1999).
22. Duo, I., Levy-Clement, C., Fujishima, A., & Comninellis, C. Electron Transfer Kinetics on Boron-Doped Diamond Part I: Influence of Anodic Treatment. *Journal of Applied Electrochemistry.* **34** (9), 935-943 (2004).
23. Mahé, E., Devilliers, D., & Comninellis, C. Electrochemical reactivity at graphitic micro-domains on polycrystalline boron doped diamond thin-films electrodes. *Electrochimica Acta.* **50** (11), 2263-2277 (2005).
24. Vandenabeele, P. *Practical Raman spectroscopy: an introduction.* John Wiley & Sons (2013).
25. Filik, J. Raman spectroscopy: a simple, non-destructive way to characterise diamond and diamond-like materials. *Spectroscopy Europe.* **17** (5), 10 (2005).
26. Tuinstra, F., & Koenig, J. L. Raman Spectrum of Graphite. *The Journal of Chemical Physics.* **53** (3), 1126-1130 (1970).
27. Tachibana, T., Williams, B., & Glass, J. Correlation of the electrical properties of metal contacts on diamond films with the chemical nature of the metal-diamond interface. II. Titanium contacts: A carbide-forming metal. *Physical Review B.* **45** (20), 11975 (1992).
28. Zivcova, Z. V., *et al.* Electrochemistry and *in situ* Raman spectroelectrochemistry of low and high quality boron doped diamond layers in aqueous electrolyte solution. *Electrochimica Acta.* **87**, 518-525 (2013).
29. Granger, M. C. *et al.* Standard Electrochemical Behavior of High-Quality, Boron-Doped Polycrystalline Diamond Thin-Film Electrodes. *Analytical Chemistry.* **72** (16), 3793-3804 (2000).
30. Bard, A. J., & Faulkner, L. R. *Electrochemical methods. Fundamentals and Applications.* 2nd ed., John Wiley and Sons (2001).
31. Simonov, A. N. *et al.* Inappropriate Use of the Quasi-Reversible Electrode Kinetic Model in Simulation-Experiment Comparisons of Voltammetric Processes That Approach the Reversible Limit. *Analytical Chemistry.* **86** (16), 8408-8417 (2014).

32. Terashima, C., Rao, T. N., Sarada, B. V., Spataru, N., & Fujishima, A. Electrodeposition of hydrous iridium oxide on conductive diamond electrodes for catalytic sensor applications. *Journal of Electroanalytical Chemistry.* **544**, 65-74 (2003).
33. Bitziou, E., O'Hare, D., & Patel, B. A. Simultaneous Detection of pH Changes and Histamine Release from Oxyntic Glands in Isolated Stomach. *Analytical Chemistry.* **80** (22), 8733-8740 (2008).
34. Pickup, P. G., & Birss, V. I. The kinetics of charging and discharging of iridium oxide films in aqueous and non-aqueous media. *Journal of Electroanalytical Chemistry and Interfacial Electrochemistry.* **240** (1-2), 185-199 (1988).
35. Baur, J. E., & Spaine, T. W. Electrochemical deposition of iridium (IV) oxide from alkaline solutions of iridium(III) oxide. *Journal of Electroanalytical Chemistry.* **443** (2), 208-216 (1998).
36. Carmody, W. R. Easily prepared wide range buffer series. *Journal of Chemical Education.* **38** (11), 559 (1961).
37. Glab, S., Hulanicki, A., Edwall, G., & Ingman, F. Metal-Metal Oxide and Metal Oxide Electrodes as pH Sensors. *Critical Reviews in Analytical Chemistry.* **21** (1), 29-47 (1989).
38. Burgot, J.-L. *Ionic equilibria in analytical chemistry.* Springer Science & Business Media. (2012).
39. Joseph, M. B. *et al.* Fabrication Route for the Production of Coplanar, Diamond Insulated, Boron Doped Diamond Macro- and Microelectrodes of any Geometry. *Analytical Chemistry.* **86** (11), 5238-5244 (2014).
40. Vanhove, E. *et al.* Stability of H-terminated BDD electrodes: an insight into the influence of the surface preparation. *physica status solidi (a).* **204** (9), 2931-2939 (2007).
41. Salazar-Banda, G. R. *et al.* On the changing electrochemical behaviour of boron-doped diamond surfaces with time after cathodic pre-treatments. *Electrochimica Acta.* **51** (22), 4612-4619 (2006).
42. Gelderman, K., Lee, L., & Donne, S. W. Flat-Band Potential of a Semiconductor: Using the Mott-Schottky Equation. *Journal of Chemical Education.* **84** (4), 685 (2007).
43. Ushizawa, K. *et al.* Boron concentration dependence of Raman spectra on {100} and {111} facets of B-doped CVD diamond. *Diamond and Related Materials.* **7** (11-12), 1719-1722 (1998).
44. Chrenko, R. Boron, the dominant acceptor in semiconducting diamond. *Physical Review B.* **7** (10), 4560 (1973).
45. Uzan-Saguy, C. *et al.* Hydrogen diffusion in B-ion-implanted and B-doped homo-epitaxial diamond: passivation of defects vs. passivation of B acceptors. *Diamond and Related Materials.* **10** (3-7), 453-458 (2001).
46. Hammerich, O., & Speiser, B. *Organic Electrochemistry, Fifth Edition.* Taylor & Francis (2015).
47. Juang, R.-S., & Wang, S.-W. Electrolytic recovery of binary metals and EDTA from strong complexed solutions. *Water Research.* **34** (12), 3179-3185 (2000).
48. Byrne, R. H., Kump, L. R., & Cantrell, K. J. The influence of temperature and pH on trace metal speciation in seawater. *Marine Chemistry.* **25** (2), 163-181 (1988).
49. Schonberger, E., & Pickering, W. The influence of pH and complex formation on the ASV peaks of Pb, Cu and Cd. *Talanta.* **27** (1), 11-18 (1980).
50. Chau, Y., & Lum-Shue-Chan, K. Determination of labile and strongly bound metals in lake water. *Water Research.* **8** (6), 383-388 (1974).

